Exciton Relaxation and Transfer in the LH2 Antenna Network of Photosynthetic Bacteria

Arvi Freiberg,*,†,‡ Kõu Timpmann,†,‡ Su Lin,† and Neal W. Woodbury†

Department of Chemistry and Biochemistry and Center for the Study of Early Events in Photosynthesis, Arizona State University, Tempe, Arizona 85287, and Institute of Physics, University of Tartu, EE2400 Tartu, Estonia

Received: May 18, 1998; In Final Form: October 19, 1998

Exciton relaxation and energy-transfer processes in the circular B800−850 light-harvesting (LH2) complex from the purple nonsulfur photosynthetic bacterium *Rhodobacter sphaeroides* were studied at 8 K. Excitons were selectively excited in the B850 aggregate of bacteriochlorophyll *a* molecules by 5 nm spectral bandwidth, 150 fs duration pump pulses tuned over the whole B850 ground-state absorption spectrum (between 820 and 880 nm). The transient absorption spectra were measured over a 140 nm spectral range using a white-light continuum probe pulse. A strong effect of transient spectral hole burning was observed, with the shape of the transient spectrum being pump wavelength dependent. A single, very narrow bleaching line was observed when the sample was pumped in the region between 840 and 850 nm. Spectra using excitation outside of this wavelength region revealed a more complex structure. The time evolution of the transient spectra in the femtosecond and picosecond time range was both pump and probe wavelength dependent, with time-dependent changes being least notable at far-red excitation. A model was put forward to interpret the data, assuming that the sample consists of an ensemble of spectrally disordered excitons, each representing a separate B850 ring. The model takes into account a dimeric association of the bacteriochlorophyll molecules in the B850 ring and necessarily includes, besides nearest-neighbor transition dipole−dipole couplings, also the nonnearest-neighbor couplings. We conclude that all the observations of the present work and many others in the literature can be satisfactorily explained in terms of this spectrally disordered exciton model. Specifically, (i) the pump wavelength dependence of the shape of transient spectra is due to exciton-site selection within the ensemble of disordered excitons, and (ii) the ultrafast spectral dynamics is due to interexciton state relaxation (characteristic time constant 130 fs) and exciton transfer between different B850 complexes (several time constants spanning from a picosecond to a subnanosecond time range). From the comparison with the experiment, the following model parameters emerge: effective nearest-neighbor exciton coupling energy, $V = 350$ cm^{-1}; full width at half-maximum of the Gaussian inhomogeneous distribution function of site energies, $\Gamma_{inh} = 600$ cm^{-1}; average decay time-limited homogeneous width of the upper exciton levels, $\Gamma = 42$ cm^{-1} and the lowest level, $\Gamma_0 = 3.5$ cm^{-1}; mean transition energy of the basic heterodimer of the B850 ring, $\nu_0 = 12\,420$ cm^{-1}; average exciton delocalization size in the B850 ring, $N_{coh} = 5$ bacteriochlorophyll molecules.

1. Introduction

In photosynthetic membranes, antenna (bacterio) chlorophyll−protein complexes serve to carry out very efficient light energy collection and transfer into the photochemical reaction center. The exact nature of the antenna excitations has been studied for many years but remains a matter of considerable debate. The possibility that the excitation might exist as an exciton, delocalized over several chlorophyll molecules, was first put forward already in the late 1930s.[1] Despite the physical attractiveness of the exciton idea, the experimental evidence has been limited as yet (for a review, see ref 2). One reason for this is the usually strong inhomogeneous broadening of in vivo (bacterio) chlorophyll spectra[3−5] that tends to obscure the exciton effects.

Recently, high-resolution structural data for photosynthetic pigment−protein complexes has become available.[6,7] This has made possible a more sophisticated analysis of this problem. It has been found that in purple photosynthetic bacteria the peripheral (LH2) antenna units have a simple ringlike structure. The LH2 accommodates two rings of bacteriochlorophyll *a* (BChl) molecules, B800 and B850, labeled according to their major long-wavelength Q_y absorption maxima at about 800 and 850 nm, respectively. The B850 ring includes 18 or 16 (depending on the species) BChl molecules in a tilted face-to-face or waterwheel-like arrangement. B800 is, correspondingly, an array of 9 or 8 BChls in a side-by-side arrangement.

There is a general understanding that the electronic excitations in the B850 rings are delocalized to some extent even at room temperature. The delocalized exciton states are properties of a molecular group, not a single molecule. The structural bases of this viewpoint is a very dense packing of the BChl molecules in the B850 array, which have a center-to-center distance of about 0.9−1.0 nm and a geometry favoring strong coupling.[8] In the B800 ring, the situation is different. There, the distance between adjacent B800 molecules is 2.1−2.2 nm, coupling is about an order of magnitude weaker,[8] and the excitations are considered more or less localized initially on a single B800

* Author to whom correspondence should be addressed at the University of Tartu. E-mail: freiberg@fi.tartu.ee. Phone: +372-7-383024. Fax: +372-7-383033.

† Arizona State University.

‡ University of Tartu.

10.1021/jp982265u CCC: $15.00
Published on Web 12/08/1998

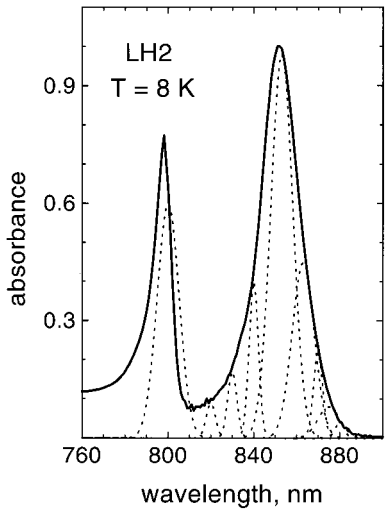

Figure 1. Inhomogeneously broadened steady-state absorption spectrum of LH2 antenna complexes at 8 K (highlighted with bold continuous curve). Superimposed are Gaussian spectra of pump pulses with their peaks at 820, 830, 840, 853, 863, 870, 875, and 880 nm, the excitation wavelengths applied in the present work. The excitation pulse spectral bandwidths (fwhm) are 5 or 12 nm.

molecule. A consensus is lacking, however, when the more detailed properties of excitons in the B850 ring are considered, including the question of how excitons show up in the overall light-harvesting dynamics. More specifically, both theoretical and experimental arguments have been raised supporting a variety of exciton coherence sizes at room temperature ranging from 2[9] to 18,[10] i.e., the whole ring of the BChl molecules. Accordingly, the proposed resonance coupling energy varies over a large range, between about 100 and 800 cm^{-1}.

Recently, we performed low-temperature (18 K) transient absorbance measurements using a series of relatively narrow (7 nm full width at half-maximum, fwhm) excitation pulses resonant with the long-wavelength side of the inhomogeneously broadened B850 ground-state absorption spectrum and probing over a broad range of wavelengths.[11] The data could be interpreted in terms of substantial heterogeneity between rings of the LH2 complexes. The rings that absorb near the center of the 850 nm absorption band of LH2 seem to be closer to ideal, meaning that their ring symmetry is almost perfect. Excitation of this population results in a single bleaching band. With time, the excitons relax and migrate to the lower energy rings near the red edge of the absorption band. These rings are significantly disturbed and their spectrum is different. Therefore, the shape of the transient spectrum changes significantly at later times. If one excites near the red edge of the 850 nm absorption band, one is directly exciting strongly disturbed rings and a characteristic two-peak shape of the spectrum is resolved initially upon excitation.

The above model suggests that there should also be a population of disturbed LH2 rings with their absorption spectrum edge shifted to the blue relative to the center of the B850 absorption band. This suggestion is indeed confirmed by the present work, which constitutes a systematic study of exciton relaxation and energy-transfer dynamics in the *Rhodobacter (Rb.) sphaeroides* mutant membranes that include only LH2 antenna proteins and are devoid of the core LH1 antenna and reaction center proteins.[12] The same uncertainty-principle-limited transient absorption technique as described in ref 11 was utilized with the following significant improvements. (i) The excitation pulses have been tuned over the whole B850 ground-state absorption band (see Figure 1). For comparison, data were also recorded using nonselective excitation, resonant with the B800 absorption band. (ii) Reducing the spectral pulse width to 4−5 nm increased the spectral selectivity of the measurements. (iii) The temperature was reduced to 8 K to minimize the homogeneous width of exciton levels. (iv) Application of a state of the art laser system based on the all-solid-state Ti:sapphire laser technology dramatically improved the signal-to-noise ratio of the data.

2. Excitons in Circular Arrays of Two-Level Molecules

Here, we review the properties of excitons in an idealized circular aggregate of N identical organic molecules.[13−15] If the direct overlap between the monomer molecular orbitals is negligible, then the exciton interaction can be expressed as the interaction between the transition densities of the monomer units in the aggregate. When the size of the monomer is small compared to the distance between the monomers, the exciton interaction can be reduced to the interaction between the transition dipole moments.[16] Further, commonly used simplifications are the two-level model, the nearest-neighbor approximation, and the neglect of electron−phonon and electron−vibrational couplings. The two-level model applies when the transition under consideration is energetically well separated from the rest of the transitions. Neglecting of the electron−phonon and electron−vibrational couplings is appropriate if the exciton coupling energy and splitting between the exciton levels is large compared to the dephasing-induced widths of the levels and to the exciton−phonon/exciton−vibrational coupling energy. The applicability of the nearest-neighbor approximation is less well defined. It needs to be checked specifically based on the real structure of the aggregate, because not only distance but also relative orientation of the transition dipoles of the monomer units plays an important role in determining the strength of the exciton interaction (see eq 2 below). Within the above approximations, the effective Hamiltonian of the aggregate can be represented as

$$H = \Delta_0 \sum_i |i\rangle\langle i| + \sum\sum_{i,j(i\neq j)} V_{ij} |j\rangle\langle i| \qquad (1)$$

Here, Δ_0 is the localized monomer (site) transition energy, $|i\rangle$ denotes the state in which the molecule i in the aggregate is excited and the summations are over all N molecules of the aggregate. V_{ij} is the resonant coupling energy between the molecules i and j, which in the point-dipole approximation (if measured in cm^{-1} units) is given as

$$V_{ij} = 5.04 \mu_i \mu_j \kappa / \epsilon R^3 \qquad (2)$$

In eq 2, the orientation factor κ is defined as

$$\kappa = (\mathbf{e}_i \cdot \mathbf{e}_j) - 3(\mathbf{e}_i \cdot \mathbf{e}_{ij})(\mathbf{e}_j \cdot \mathbf{e}_{ij}) \qquad (3)$$

where $\mathbf{e}_i$, $\mathbf{e}_j$ and $\mathbf{e}_{ij}$ are the unit vectors along the transition dipoles in the monomers i and j and the line joining the two dipole centers, respectively; ϵ is the dielectric constant of the medium (relative permittivity); R is the separation of the transition dipoles measured in nanometers; $\mu_{i,j}$ are the corresponding monomer transition dipole moments in debye units. As a result of resonant coupling (the nondiagonal elements of the effective Hamiltonian matrix (1)), the site excitations are nonstationary in the aggregate. Diagonalization of the Hamiltonian (1) gives eigenenergies of the stationary states of the aggregate or exciton states. For the simple Hamiltonian (1) with only nearest-neighbor interactions, V, the quantified exciton energies can be calculated as

$$E_k = \Delta_0 + 2V\cos(2\pi k/N) \quad (4)$$

Here k takes N integer values, 0, ±1, ±2, etc. Thus, the N-fold degenerate aggregate state of noninteracting monomers splits into a manifold of exciton levels from which most are 2-fold degenerate. The exciton levels span over the energy range roughly equal to 4 times the resonant coupling energy, V. The exciton state $|\Phi_k\rangle$ is a coherent superposition of the excited states of the sites,

$$|\Phi_k\rangle = \sum_i a_{ki}|i\rangle \quad (5)$$

where a_{ki} are the $|\Phi_k\rangle$ exciton state eigenvector components. They specify the amplitude of each site's contribution to the exciton state. The intensity of the exciton spectral line is proportional to the modulus square of the exciton transition dipole moment, μ_k.

$$\mu_k = \sum_i a_{ki}\mu_i \quad (6)$$

The circular symmetry of the aggregate determines that in general only the three lowest, $k = 0$ and $k = \pm 1$ exciton states are optically accessible. If the transition dipoles lay on the ring surface, only the $k = \pm 1$ transitions have oscillator strength. Besides the described so-called one-excitons, also two-excitons, three-excitons, etc., up to N-excitons exist, according to the number of simultaneously excited sites in the aggregate.[17] Optical transitions are only possible between the bands differing by a single exciton.

Unfortunately, the structure of the B850 BChl ring is too complex to be accurately described by this simple model. For example, in *Rhodopseudomonas acidophila*, the ring is constructed from nine α,β polypeptide pairs, each of which noncovalently binds a pair of BChl molecules with a 0.96 nm nearest-neighbor distance.[6] The nearest-neighbor distance between BChls from the neighboring polypeptide couple is 0.89 nm leading to a slightly different interaction energy.[8] The Q_y transition dipoles of individual molecules are almost tangential to the ring and antiparallel within each dimer.[6−8] The BChls in a dimer are not equivalent because they are associated with different polypeptides (α or β) and one of the BChls is noticeably distorted from planarity.[6]

Excitons in a circular chain of heterodimers have been considered in ref 18. There are some important differences when compared with simple cyclic aggregates. The one-exciton state consists of two branches of exciton manifolds arranged symmetrically relative to the mean of the heterodimer site energies Δ_1 and Δ_2. The phenomenon is known as Davydov splitting.[19] In the nearest-neighbor approximation, the $2N$ exciton level energies (N here denotes the number of dimers in the chain) are given by[20]

$$E_k = (\Delta_1 + \Delta_2)/2 \pm \{[(\Delta_1 - \Delta_2)/2]^2 + V_1^2 + V_2^2 + 2V_1V_2\cos[2\pi k(d_1 + d_2)/N]\}^{1/2} \quad (7)$$

In eq 7, $-N/2 \le k \le N/2$, V_1 and V_2 represent the nearest-neighbor resonant interaction energy within the heterodimer and between the dimers, respectively, and d_1 and d_2 are the corresponding distances. It follows from eq 7 that the lowest energy level is located at $(\Delta_1 + \Delta_2)/2 - \{[(\Delta_1 - \Delta_2)/2]^2 + (V_1 + V_2)^2\}^{1/2}$, whereas the highest level is at $(\Delta_1 + \Delta_2)/2 + \{[(\Delta_1 - \Delta_2)/2]^2 + (V_1 + V_2)^2\}^{1/2}$. The two Davydov submanifolds are separated by an energy gap equal to $2\{[(\Delta_1 - \Delta_2)/2]^2 + (V_1 - V_2)^2\}^{1/2}$. As seen, the heterodimer transition energy mismatch changes the total width of the exciton spectrum and also increases the size of the energy gap between the Davydov submanifolds. The gap is present also in the case of homodimers with equal dimer site energies, but only when the coupling energies are different. Equation 4 is recovered from eq 7 if $\Delta_1 = \Delta_2 \equiv \Delta_0$ and $V_1 = V_2 \equiv V$, i.e., when the symmetry of the homogeneous ring is restored.

As a result of the geometrical constraint that the dipole moments of the two BChls in the B850 heterodimer are almost exactly antiparallel, the lower Davydov manifold carries almost all the absorption intensity. Furthermore, as all the transition dipoles are orientated almost on the ring surface, most of the oscillator strength is concentrated into the two next lowest ($k = \pm 1$) degenerate transitions. It was estimated in refs 8, 18, and 21−23 that if all the BChls were identical and their Q_y transition dipoles oriented as was determined in ref 6, the transition to the lowest ($k = 0$) exciton state would carry not more than 1−2% of the total oscillator strength.

3. Experimental Section

Isolation of Chromatophores and Sample Handling. Cultures of a *Rb. sphaeroides* strain with deleted core antenna LH1 and reaction center genes were grown semiaerobically in a rich medium as previously described.[12] After being harvested, the cells were resuspended in TEN (15 mM Tris-HCl, pH 8, 1 mM EDTA, 0.1 M NaCl), and the cells were lysed at 20 000 psi in a French pressure cell. The cell extracts were incubated with DNAse and then centrifuged for 30 min at 8000 rpm (Sorvall GS3 rotor) to remove whole cells and debris. The membranes were isolated by high-speed (45 000 rpm) centrifugation for 2 h 45 min (Beckman Ti45 rotor) on a 0.3, 0.6, and 1.2 M sucrose step gradient containing TEN. The chromatophore preparations were suspended in a TEN buffer at pH 8.0 giving a final optical density of about 20 at 850 nm measured in a standard cell of 1 cm optical path length.

Per 1 vol of sample and buffer, 2 vols of glycerol were added. The protein solution was then fixed between two fused quartz plates about 1.2 mm apart and slowly cooled to 8 K in a coldfinger-type closed-cycle helium cryostat from APD Cryogenics.

Sample cracking upon cooling below 130−140 K was avoided by coating the inner surfaces of the sample cell plates with Repel-Silane (a solution of dimethyldichlorosilane in trichloroethane) as was described in ref 24. Careful degassing of the protein solution and the use of freshly prepared sample also helps to improve the quality of the low-temperature sample glass. With these precautions in sample preparation, it was possible to record transient spectra across the spectral region of excitation without major scattering artifacts.

Femtosecond Transient Absorption Spectrometer. A diagram of the transient absorbance instrument is presented in Figure 2. A commercially available Ti:sapphire oscillator/regenerative amplifier combination (Clark-MXR model CPA-1000) was used as a source of femtosecond light pulses. The amplifier operated at a 1 kHz repetition rate and produced approximately 100 fs pulses at 775 nm with a pulse energy of 0.9 mJ. The source pulses were split using a 10% beam splitter. The stronger pulse beam was used to generate tunable pump pulses in an optical parametric amplifier (OPA-Clark MXR) in the broad wavelength region from 550 nm to 1.5 μm. The spectral bandwidth of the OPA pulses was 12−15 nm. Bandpass interference filters with fwhm of 5 nm (Omega Optical) were used for further narrowing the spectral profile of the OPA pulses. As a result, the temporal width of the pump pulse was

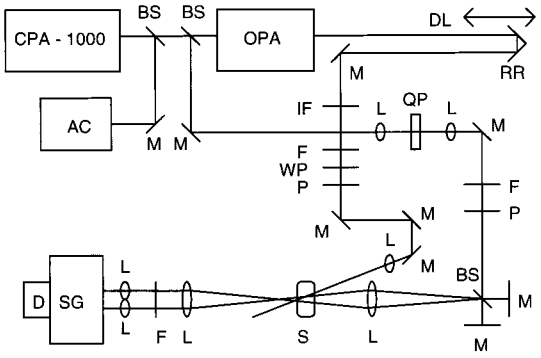

Figure 2. Diagram of the femtosecond transient absorption spectrometer. Abbreviations used are as follows: CPA-1000, Ti:sapphire oscillator/regenerative amplifier; OPA, optical parametric amplifier; AC, autocorrelator; SG, spectrograph; D, detector; BS, beam splitter; DL, delay line; M, mirror; RR, retroreflector; L, lens; F, filter; IF, interference filter; P, polarizer; WP, half-wave plate; QP, quartz plate; S, sample.

limited by the uncertainty principle to approximately 150 fs. These pulses were used for excitation. The probe and reference pulses were generated by sending the remaining 10% of the output from the Ti:sapphire amplifier through a 1.2 cm rotating quartz plate to generate a spectral continuum. The pump and probe beams were polarized at the "magic angle", 54.7° relative to each other. The stepping motor driven delay line controlled the variable time delay between the probe/reference and pump pulses. Various scanning lengths from 3 ps to 1 ns were utilized in order to record both fast and slow kinetics. A SpectraPro-275 spectrograph (Acton Research) equipped with a dual array CCD detector (ST-121 from Princeton Instruments) recorded the transient spectra with 1 nm resolution over the 140 nm wide probe spectral range.

The transient (differential) absorption spectrum is defined as the transient change in probe absorption caused by the pump pulse. Accordingly, the spectra at different delay times t were calculated as

$$\Delta\mathrm{OD}(\lambda,t) = \log[T_r(\lambda,t)/T_p(\lambda,t)] \qquad (8)$$

where $T_{p,r}(\lambda,t)$ is the sample transmission spectrum at probe (p) or reference (r) channels.

Data Analysis. The data were analyzed using MathSoft Mathcad 7, Origin 5.0 (Microcal Software), SigmaPlot 4.0 (SPSS), and Spectra Solve (LasTek, Australia) packages as well as a home-written global analysis routine based on the MATLAB program from Mathworks.

4. Experimental Results

Evidence for Transient Spectral Hole Burning. Figure 3 presents the initial shape of the transient absorption spectra excited using five different pump wavelengths (820, 830, 840, 870, and 880 nm) within the Q_y absorption band of the LH2 complexes. Initial means the first time when the signal was significantly larger than the background noise level. At all excitation wavelengths the pump pulse spectral width was similar, about 5 nm. If coherent coupling artifacts can be neglected, the transient absorption spectrum may be considered as a sum of excited-state absorption (ESA), stimulated emission (SE), and ground-state bleaching (GSB) subspectra. The transient absorption spectra are traditionally displayed in a way that the contribution of ESA has a positive sign (absorption increase), whereas the contributions of GSB and SE have negative signs (absorption decrease or bleaching of the sample).

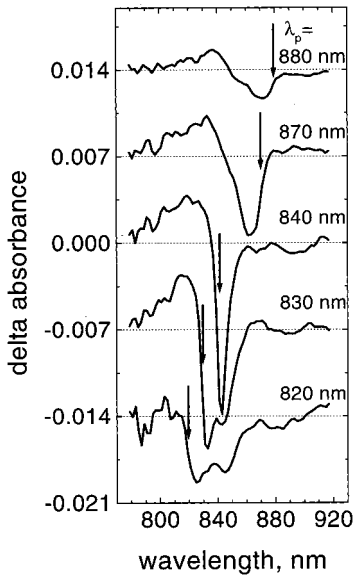

Figure 3. Dependence of the initial transient absorption band shape on the pump wavelength (the excitation wavelength, λ_p, indicated with an arrow) at 8 K. For a better observation, different spectra are shifted relative to each other vertically by a fixed absorbance. The spectral bandwidth of the pump pulse is about 5 nm. The spectra are recorded with a resolution of 1 nm at the following delay times: −540 fs (820 nm excitation); −590 fs (830 nm); −590 fs (840 nm); −200 fs (870 nm); −160 fs (880 nm).

The spectra in Figure 3 are much more structured than the time-integrated ground-state absorption spectrum shown in Figure 1. The shape of the initial difference spectrum varies considerably and in a rather systematic way with pump wavelength. When excitation is close to the red edge of the ground-state absorption spectrum, the GSB/SE difference spectrum reveals a characteristic shape observed previously in ref 11 with a shoulder at the high-energy side. The bleaching band shifts to the blue, and the initial difference spectrum becomes gradually narrower when the pump wavelength is tuned closer to the maximum of the ground-state absorption spectrum (see the spectrum measured with 870 nm excitation in Figure 3). With the excitation wavelength between 840 and 850 nm, a remarkably narrow band emerges. By studying the neighboring spectra with larger separation between the excitation peak and the maximum of the GSB/SE band, one may conclude that this probably is not due to contributions to the signal from excitation coherence artifacts. The GSB/SE band broadens again and eventually splits into two subbands when the pump wavelength is shifted to the blue from about 840 nm. The splitting increases gradually and the band shape becomes even more complex when pump wavelengths further to the blue are used. Taking into account the fact that the initial spectra are much narrower than the ground-state absorption spectrum of Figure 1, the effects described are apparently a consequence of the spectral inhomogeneity of the antenna system.

It is also instructive to note the following. (i) The characteristic excitation wavelength range (denoted as $\lambda_{\pm1}$, the meaning of the subscript will become clear later) where the initial transient differential spectrum appears as a single, narrow bleaching signal is blue-shifted relative to the ground-state absorption spectrum maximum at about 852 nm (Figure 1). (ii) When excitation at wavelengths longer than $\lambda_{\pm1}$ is used, most of the bleaching appears to the blue of the peak of the pump. In contrast, when exciting at wavelengths shorter than $\lambda_{\pm1}$, bleaching appears predominantly to the red from the pump pulse. (iii) The precise shape of the GSB/SE spectra obtained with

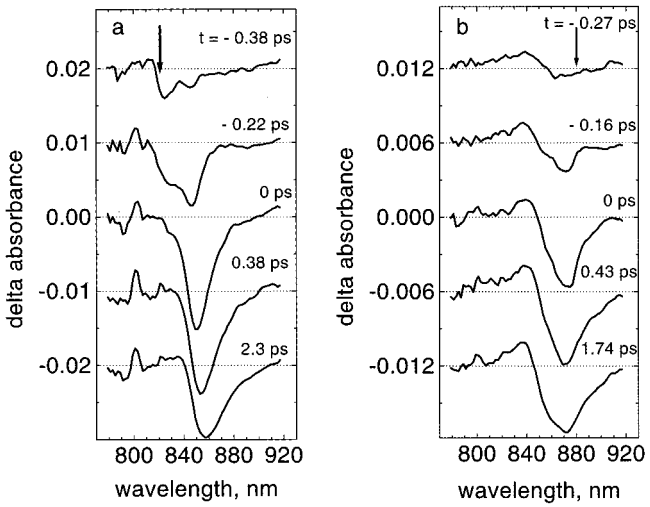

Figure 4. Transient absorption spectra recorded at the different delay times indicated. Time zero is defined at the maximum of the bleaching peak. Excitation is at (a) 820 and (b) 880 nm. Other conditions and conventions are as in Figure 3.

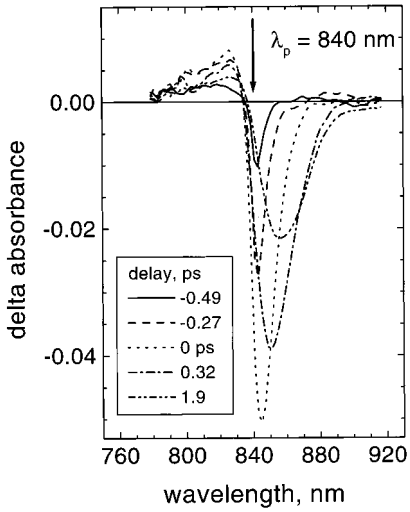

Figure 5. Transient absorption spectra excited at 840 nm and recorded at the different delay times indicated. Other conditions are as in Figures 3 and 4.

pump pulses symmetrically shifted to the red and to the blue from the $\lambda_{\pm 1}$ range is different. When using blue side excitation, the lower energy bleaching subband appears almost always to be resonant with the $\lambda_{\pm 1}$ region. In contrast, the use of red edge excitation results in the upper energy subband being considerably red shifted compared to the $\lambda_{\pm 1}$ range (compare, for example, the spectra measured with 830 and 880 nm excitation in Figure 3). (iv) There is a gradual increase of intensity of the ESA component relative to the GSB/SE bleaching counterpart when the pump wavelength is tuned from the blue edge of the ground-state absorption spectrum to its red edge. In Figure 3, it can be seen that the ESA is nearly absent with 820 nm excitation, whereas it is rather prominent with 880 nm excitation. The present results agree and complement the earlier reported data.[11]

Dynamics of Spectrally Selected Transient Spectra. It was shown in our earlier work [11] that the most dramatic spectral changes take place within a couple of picoseconds after excitation. Therefore, we shall mainly concentrate on the short-time dynamics here, although the actual measurements were done at probe pulse time delays up to a nanosecond after excitation. Notice that here and below, the time labeled zero is arbitrarily defined as the moment at which the bleaching signal reaches its maximum.

Figure 4 shows the transient absorption spectra of LH2 complexes with 820 and 880 nm excitation, i.e., at opposite edges of the ground-state absorption spectrum. The behavior of the spectrum using 880 nm excitation (Figure 4b) is very similar to that described in ref 11 using 875 nm excitation. Briefly, the temporal changes of the spectral shape are minor. They include some ultrafast intensity redistribution between the doublet components in favor of the lowest energy band and emergence of an extra negative band near 900 nm, which grows in behind the redmost GSB/SE peak. There is also a 2−3 nm red shift of the whole spectrum within about 2 ps. The temporal behavior of the spectra is quite different with short-wavelength 820 nm excitation (Figure 4a). The most striking ultrafast variations include complete disappearance of the higher energy component of the two-peak structure and a huge (over 30 nm within 2 ps) red shift of the entire spectrum. The lower energy GSB/SE peak initially (at $t = -0.38$ ps) in the $\lambda_{\pm 1}$ region shifts to the red with time. A considerable broadening of the spectrum accompanies this red shift. As noted above, the ESA is initially very weak using short-wavelength excitation, but it grows stronger with time.

As shown in Figure 3, only a single, narrow GSB/SE band is observed with 840 nm excitation. The initial spectral width of this band is apparently limited by the width of the excitation pulse. Figure 5 follows further time evolution of the band. While the band's central position is conserved for quite some time (during about 500 fs) before it shifts to the red, the band starts to broaden from the very beginning. The broadening is strongly asymmetric, mostly toward the long-wavelength side of the spectrum.

Pump and Probe Wavelength-Dependent Ultrafast Kinetics. The overall dependence of the kinetics on pump and probe wavelengths was noted previously in ref 11. Here, we shall focus on the short-time kinetics, which could be better studied using the present Ti:sapphire-based transient absorbance apparatus because of superior stability. The observed kinetics is in general nonsingle exponential. The fastest kinetics are recorded with short-wavelength excitation and at the peak of the GSB/SE spectrum. Again, the fact that the maximum wavelength of transient bleaching does not, in most cases, coincide with the pump pulse spectrum strongly argues against the possibility that the ultrafast kinetics observed are due to an excitation coherent artifact.

Figure 6 demonstrates two typical kinetic traces measured with the relatively short-wavelength 840 nm excitation. The appearance and decay of the bleaching at 839 nm is extremely rapid, with the initial kinetics being limited by the pump pulse temporal shape. A multiexponential analysis of the bleaching recovery kinetics returns two components with lifetimes of 135 ± 20 fs and roughly 1 ps. The kinetics is rather different when the system is probed at wavelengths that are long compared to the excitation wavelength, e.g., at $\lambda_{pr} = 871$ nm, as shown in Figure 6. There, the bleaching is visibly retarded compared to the rising front of the pump pulse. The signal appears with a roughly 100 fs time constant. Thus, the fastest bleaching recovery time constant at shorter wavelengths and the time constant with which the bleaching signal appears at longer wavelengths are nearly the same considering the experimental error. This correlation is most probably not accidental and is a reflection of the downward exciton energy relaxation processes, as will be discussed below.

Using long-wavelength (880 nm) excitation, the kinetics is almost insensitive to the probe wavelength and is rather similar

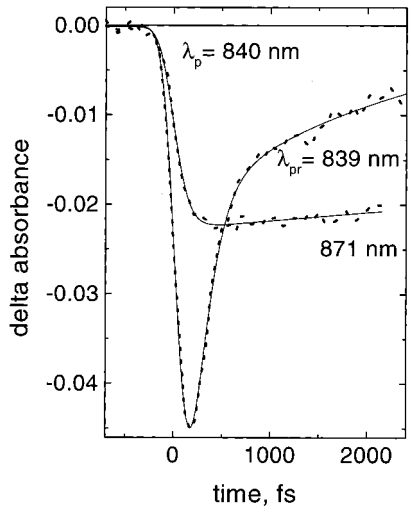

Figure 6. Short-time kinetics of the absorbance change recorded at 839 and 871 nm. The solid lines represent exponential fits of the data that is shown in dotted lines. Excitation was at 840 nm. See text for details.

to the 871 nm probe kinetics shown in Figure 6 without initial fast bleaching recovery. (Data not shown. The interested reader may consult ref 11 where it is shown that the average rate of the bleaching recovery tends to decrease with increasing pump wavelength.) However, with 880 nm excitation, no retardation is observed in the appearance of the 871 nm signal; the bleaching signal increases concurrently with the pump pulse.

5. Discussion

The observed transient spectral hole burning is a clear indication of spectral heterogeneity in the LH2 antenna system. An important question is whether this heterogeneity reflects the distribution of different BChl molecules within a single LH2 complex (more specifically, within a B850 ring) or the distribution of different LH2 complexes (heterogeneity between B850 rings). To answer this question, we shall first consider the primary consequences of diagonal (spectral) disorder on the spectral properties of excitons in an ensemble of circular molecular aggregates.

Excitons in Disordered Circular Aggregates: A Model. Excitons in simple (one molecule per unit cell) circular aggregates
with diagonal disorder have been well studied previously.[9,13−15,21−23,25,26] In the lowest order approximation of perturbation theory, the main differences of introducing diagonal disorder compared to the idealized circular aggregate model described in Section 2 are as follows.[21] (i) All exciton levels shift uniformly by an energy σ/N (σ is the antenna site energy defect). (ii) The degeneracy of the exciton levels is lifted. The levels split by $2|\sigma/N|$. (iii) With increasing disorder, the lowest energy $k = 0$ state becomes progressively more dipole allowed due to mixing with the strong dipole-allowed $k = \pm 1$ states. The dipole strength of the transition to the lowest state increases as $2(\mu_1|\sigma/N|/\Delta E_{10})^2$ (μ_1 is the dipole moment of the $k = \pm 1$ transition, and ΔE_{10} is the energy gap between the $k = \pm 1$ and $k = 0$ levels). The dipole strength of the higher, $k > \pm 1$, transitions increases as $(2\ \mu_1|\sigma/N|/\Delta E_{k1})^2$.

It should be noticed that perturbation theory is limited to only a small range of the site energy defect parameter, σ, relative to the nearest-neighbor coupling energy, V. A more realistic approach based on numerical modeling of a cyclic Frenkel-exciton aggregate with energetic disorder has been developed in refs 15, 22, 23, and 25−27. A similar numerical description of the one-exciton spectrum of an ensemble of disordered ring aggregate of nine heterodimers is adopted here. Exciton level energies in every B850 ring are calculated as eigenenergies of the effective Hamiltonian (1), except that the diagonal elements of the matrix representing the Q_y transition energies of individual BChls are all different. We assume that the offset energies, δ_i, of the transition energies, $\Delta_i = \Delta_0 + \delta_i$, follow a Gaussian distribution ($P(\delta_i)$) with zero mean and standard deviation σ (the fwhm of the distribution function is $\Gamma_{inh} \approx 2.35\sigma$), $P(\delta_i) \propto \exp(-\delta_i^2/2\sigma^2)$. We also assume that the off-diagonal elements of the effective Hamiltonian, representing resonant coupling between individual BChl molecules, do not alter their values when the diagonal matrix elements are changed. For completeness, not only nearest-neighbor but all possible dipolar interactions in the ring of 18 BChl molecules (V_{ij} in eq 1) were taken into account based on the high-resolution X-ray structure of LH2 from *Rhodopseudomonas acidophila*.[6] The interaction matrix and the coordinates of the transition dipole moment unit vectors were kindly provided to us by T. Pullerits.[27]

The algorithm for the numerical calculations of the one-exciton absorption spectrum is straightforward. By means of a random number generator, we generated an ensemble of several thousand aggregates of 18 molecules, each represented by a particular random set of transition energies. The resulting Hamiltonian was then numerically diagonalized in order to solve for the exciton energy levels and eigenvectors. The dipole strengths of k-th exciton transiton are proportional to μ_k^2 (see eq 6) and are easily obtained once the eigenvectors have been calculated. Every exciton transition is characterized by a homogeneous Lorentzian line shape, $L(E)$, subject to a normalization condition $\int L_k(E)\, dE = \mu_k^2$. For the k-th exciton transition

$$L_k(E) = (2\mu_k^2/\pi\Gamma_k)\{[2(E - E_k)/\Gamma_k]^2 + 1\}^{-1} \qquad (9)$$

Here Γ_k is the homogeneous width (fwhm) of the k-th exciton level. The major reason for homogeneous broadening of the exciton levels at low temperatures is the finite decay time of the exciton states. For simplicity, we have taken all the exciton level widths to be the same and equal to Γ, except the lowest level in every aggregate, which for physical reasons (as a last rung in the relaxation ladder), should have a much smaller width. This lowest level width is later denoted with Γ_0. The one-photon exciton absorption spectrum was finally calculated as

$$A(E) = 1/M\langle\sum_k L_k(E)\rangle \qquad (10)$$

where the angular brackets denote an average over an ensemble of M randomly generated aggregates. The sum of k runs over all eigenstates of the individual aggregate within the ensemble.

Figure 7 presents a few results of our simulation of the absorption spectrum of disordered aggregates with different σ and Γ_0 values. For ease of comparison, the relative energy scale is used, with the energy unit being the largest resonant coupling energy present in the system. Zero of the x-axis is located at the mean of the elementary heterodimer site energies. In Figure 7a, two ensembles of aggregates ($M = 2000$) with different amounts of disorder are compared. As seen, the expectations based on the perturbation theory described above are generally fulfilled. With disorder, the spectrum of the aggregate is shifted toward lower energy compared to the spectrum of the aggregate lacking disorder. Essentially, all exciton levels become optically accessible, although absorption at the top of the exciton band (around energy equal to 2) remains rather weak even in the case of relatively large disorder, $\sigma = 1$. The spectral broadening at

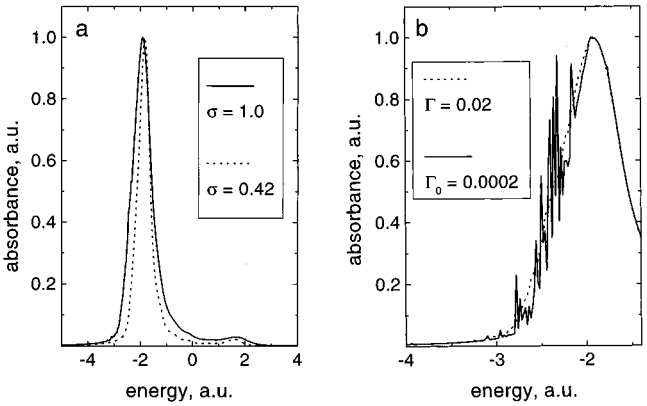

Figure 7. Simulated absorption spectra of disordered aggregates ($M = 2000$) of B850 BChls from the LH2 antenna. (a) Two ensembles of aggregates with different σ (1.0 and 0.4) but similar homogeneous exciton line widths ($\Gamma_0 = 0.02$ and $\Gamma = 0.2$). (b) Two absorption spectra of the same ensemble of disordered aggregates, calculated assuming different Γ_0 (0.2 and 0.0002). Other parameters are $\sigma = 1.0$ and $\Gamma = 0.2$.

the bottom of the exciton band (around energy equal to -2) with increasing disorder is also remarkable.

Of special interest is the contribution of the lowest energy $k = 0$ aggregate levels into the overall exciton absorption spectrum. This contribution can be revealed by assigning very small spectral width to every $k = 0$ level in the ensemble. As a result of the normalization condition, $\int L_k(E)\, dE = \mu_k^2$, the narrow $k = 0$ spectral lines gain peak intensity and become easily distinguishable on the much broader background of spectral continuum caused by transitions to the higher energy $k > 0$ exciton states. Figure 7b illustrates the case. Two absorption spectra compared in this figure belong to the same ensemble of aggregates but were calculated using vastly different Γ_0 values ($\Gamma_0 = 0.2$ and 0.0002). It can be noticed that the $k = 0$ exciton states from different aggregates contribute only to the low-energy slope of the absorption spectrum (narrow spikes are absent at around the maximum as well as at the high-energy slope of the spectrum). Although the overall shape of the absorption spectrum is strongly affected by the disorder, the position of the spectral maximum is relatively insensitive to it and is mostly determined by the $k = \pm 1$ exciton transitions, just as in an ensemble of perfectly ordered rings.

Figure 7b also contributes to understanding how the steady-state hole burning spectra are formed. As known (see refs 14 and 23), a narrow persistent hole in the B850 band of LH2 can only be burned on the low-energy slope of the absorption spectrum. The narrow hole is always accompanied on the high-energy side by a broad hole. Burning around the maximum or on the high-energy slope of the B850 band results in only a broad hole. Realizing that the narrow $k = 0$ exciton transitions contribute only to the low-energy slope of the absorption spectrum and that the hole burning efficiency is proportional to the absorbed energy at the burning laser frequency allows a qualitative understanding of the hole burning phenomenon in an ensemble of disordered excitons.

A reasonable assumption is that by using a macroscopic sample, one is dealing with the optical response of a huge variety of different B850 ring aggregates. In light of the above discussion, the ground-state absorption spectrum of such a system is formed as an incoherent superposition of individual disordered exciton spectra. The disorder, which is revealed by optical spectra, is thus between rings as well as within rings.

Numerical Simulation of the B850 Ground-State Absorption Spectrum of LH2. We recall that our numerical model has a total of four parameters: the largest resonant coupling constant, V, disorder parameter, σ, and two exciton level widths, Γ_0 and Γ. Fortunately, none of these parameters is completely free. Thus, by making the reasonable assumption that at 8 K the broadening of exciton lines due to pure dephasing is negligible and the line width is totally determined by the lifetime of the exciton state, we can set a limit for Γ^{-1} from the present kinetic measurements of $\Gamma^{-1} = 100-150$ fs. An estimate of a couple of picoseconds for Γ_0^{-1} is given by hole burning data.[14,23] The possible range of the resonant coupling energy is also limited, as was discussed in the Introduction. With these constraints taken into account, the range of parameter space that needs to be searched is dramatically reduced.

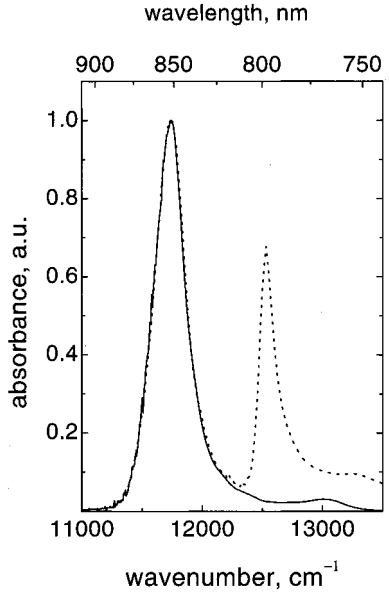

Figure 8. Simulated B850 disordered exciton absorption spectrum (continuous curve) as compared with the experimental ground-state absorption spectrum of LH2 chromatophores at 8 K (dotted curve). See text for details.

Figure 8 shows the ground-state absorption spectrum of LH2 complexes along with a simulated exciton absorption spectrum of an ensemble of disordered B850 aggregates ($M = 4000$). One can see a very good agreement between the shapes of the experimental and simulated spectra, including the long-wavelength tails. From the short-wavelength side, the comparison is limited because the experimental spectrum is obscured by the absorption of the B800 excitons. A few spikes on the long-wavelength slope of the simulated spectrum corresponding to $k = 0$ states (and absent in the experimental one) can be due either to poor statistics or to a too small Γ_0 parameter used. We shall return to this question in one of our forthcoming publications. It can be shown that the $k = 0$ states spread over a spectral range of about 500 cm^{-1}.

The following parameters were used to generate the fitting spectrum in Figure 8: $V = 350$ cm^{-1}; $\sigma = 256$ cm^{-1} (or $\Gamma_{inh} \approx 602$ cm^{-1}); $\Gamma_0 = 3.5$ cm^{-1}; $\Gamma = 42$ cm^{-1}. With these entirely reasonable parameters, the effective heterodimer transition energy is at $c/(12419\ cm^{-1}) = 805.2$ nm (c is the speed of light) and the short-wavelength edge of the B850 exciton spectrum spreads until about 770 nm.

A few comments are in order considering the fitting parameters. The fwhm of the absorption spectrum is equal to about 270 cm^{-1}; that is, it is narrowed relative to the distribution of $P(\delta_i)$ by a factor of $\Gamma_{inh}/\text{fwhm} = 2.23$. This is because delocalized exciton states average over a number of random energies, $N_{coh} = (\Gamma_{inh}/\text{fwhm})^2$. The phenomenon is referred to

as exchange narrowing[28] and allows us to estimate the average number of coherently coupled BChls in the B850 ring, $N_{coh} \approx 5$. This number is consistent with the previous estimates (see, e.g., refs 22 and 29).

A short lifetime of the lowest $k = 0$ exciton states ($\Gamma_0^{-1} \approx 1.5$ ps) can be interpreted as due to efficient energy transfer between different aggregates in the ensemble. This lifetime should entirely be considered as an average constant, because there is only a single Γ_0 parameter in our model that is the same for all aggregates. In reality, however, a broad distribution of Γ_0^{-1} lifetimes exists, including very long (sub)nanosecond lifetimes. Otherwise, it is impossible to understand the nanosecond fluorescence decay observed around the steady-state fluorescence band maximum at 880 nm,[30] as well as the slow evolution of the differential absorption spectra observed in ref 11. The energy transfer at low temperatures is predominantly toward lower energy rings and results in concentration of excitons near the red edge of the absorption band. The observed large Stokes shift between the conventional absorption and steady-state fluorescence spectra of LH2 complexes (about 370 cm^{-1} at low temperatures) is a combined result of energy transfer between different disordered aggregates in a large ensemble and of the optical selection rule for electric-dipole transitions in a single ring aggregate.

On the other hand, the lifetime of the upper exciton states revealed by modeling is $\Gamma^{-1} \approx 126$ fs, in a very good correlation with the directly measured lifetimes (see Figure 6). According to our model, this lifetime is assigned to $k > 0$ exciton states and characterizes exciton relaxation (or scattering) taking place in every single aggregate.

Exciton Site Selection. From the model calculations performed, it appears that the initial structure that is observed in the bleaching spectrum (Figure 3) is due mostly to the strong $k = \pm 1$ exciton transitions split because of the spectral disorder. The most clear-cut spectrum results when an excitation wavelength close to the maximum of the absorption spectrum is used. With this pump wavelength, predominantly the lower energy $k = 1$ states are excited. Less clear-cut structure is observed with both red- and blue-shifted excitation relative the optimum position. Using red excitation, the resolution is lost because of insufficient spectral selectivity of the pump pulse with respect to spectrally very narrow $k = 0$ transitions and overlapping of the $k = 0$ and $k = 1$ transitions from different aggregates. Using blue excitation, the structure is obscured by overlapping of different exciton transitions along with ultrafast exciton scattering, which occurs during the relatively long femtosecond pump pulse (see also ref 11).

With the pump pulse position fixed, the shape of the transient difference spectra is determined by the interplay of exciton scattering (within every aggregate) and energy transfer (between different aggregates in the ensemble). Exciton relaxation has a minor contribution when excitons are directly created at the $k = 0$ state by using red edge excitation (Figure 4b). Then, exciton transfer dominates the spectral dynamics at all times. An opposite situation is created with short-wavelength excitation, shown in Figures 4a and 5. Now, the spectral dynamics is mainly governed by exciton relaxation.

6. Concluding Remarks

The present work reinforces the importance of diagonal disorder in describing the spectral and dynamic properties of light excitations in the LH2 antenna complexes. The time dependence of the transient spectra is related to the electronic relaxation involving exciton relaxation within a complex (LH2 ring) as well as energy transfer between different complexes. The proposed model does not include nuclear relaxation. Exciton localization by phonons becomes crucial if the homogeneous line width caused by fluctuations in the transition frequency due to phonons is comparable to the exciton coupling constant.[31] Considering the coupling constant, $V = 350$ cm^{-1}, and the narrow (several wavenumbers) holes burned into the absorption profile, it seems likely that nuclear relaxation plays only a minor role in the description of LH2 complexes at low temperatures. Moreover, it has been demonstrated[32] that excitons subject to a linear exciton−phonon interaction in a harmonic lattice are described by a tight-binding Hamiltonian with diagonal Gaussian disorder, that is, formally with the same model used here. Thus, if necessary, an inclusion of vibronic coupling in the regime of weak scattering to our model is straightforward and feasible initially at the level of interpretation.

What happens with excitons at ambient temperature is a very important problem in order to understand antenna function at physiological temperatures. The fact that superradiant properties of LH2 do not change between 4 K and room temperature[22] suggests that excitons in LH2 antennas are localized due to static disorder and not due to nuclear vibrations. This also suggests that the elementary excitation relaxation and transfer processes in antenna complexes are relatively insensitive to temperature.

The transient spectra shown in Figures 3−5 demonstrate the superior information content provided by transform-limited spectroscopies compared to the traditional steady-state techniques. A variation of transform-limited transient spectroscopy in the picosecond range was introduced more than 15 years ago, and a special name, "picosecond spectrochronography", was given to it by one of the present authors.[33] By analogy, the current technique may be called femtosecond spectrochronography.

Acknowledgment. The work was performed under the U.S. Department of Agriculture Grant 96-35306-3569. A.F. and K.T. acknowledge also a partial support from the Estonian Science Foundation, Grant 2271. We thank J. Williams and J. Allen for donation of the *Rb. sphaeroides* strain with the *puf* operon deletion, J. Jackson for help in sample preparation, T. Pullerits for sharing with us of his LH2 coordinates and interaction matrix data, and R. Ruus for kind help with computer programming. This is publication no. 373 from the Arizona State University Center for the Study of Early Events in Photosynthesis.

References and Notes

(1) Franck, J.; Teller, E. *J. Chem. Phys*. **1938**, *6*, 861.

(2) van Grondelle, R.; Dekker, J. P.; Gillbro, T.; Sundstrom, V. *Biochim. Biophys. Acta* **1994**, 1087, 1.

(3) Avarmaa, R.; Rebane, K. *Spectrochim. Acta A* **1985**, *41*, 1365.

(4) Freiberg, A.; Godik, V. I.; Timpmann, K. In *Progress in Photosynthesis Research*; Biggins, J., Ed.; Martinus Nijhoff: Dordrecht, The Netherlands, 1987; Vol. 1, p 45.

(5) Timpmann, K.; Freiberg, A.; Godik, V. I. *Chem. Phys. Lett*. **1991**, *182*, 617.

(6) McDermott, G.; Prince, S. M.; Freer, A. A.; Hawthornthwaite-Lawless, A. M.; Papiz, M. Z.; Cogdell, R. J.; Isaacs, N. W. *Nature* **1995**, *374*, 517. Freer, A. A.; Prince, S. M.; Sauer, K.; Papiz, M. Z.; Hawthornthwaite-Lawless, A. M.; McDermott, G.; Cogdell, R. J. *Structure* **1996**, *4*, 449.

(7) Koepke, J.; Hu, X.; Muenke, C.; Schulten, K.; Michel, H. *Structure* **1996**, *4*, 581.

(8) Sauer, K.; Cogdell, R. J.; Prince, S. M.; Freer, A.; Isaacs, N. W.; Scheer, H. *Photochem. Photobiol.* **1996**, *64*, 564. Alden, R. G.; Johnson, E.; Nagarajan, V.; Parson, W. W.; Law, C. J.; Cogdell, R. G. *J. Phys. Chem. B* **1997**, *101*, 4667.

(9) Somsen, O. J. G.; van Mourik, F.; van Grondelle, R.; Valkunas, L. *Biophys. J.* **1994**, *66*, 1580.

(10) Leupold, D.; Stiel, H.; Teuchner, K.; Nowak, F.; Sandner, W.; Ücker, B.; Scheer, H. *Phys. Rev. Lett.* **1996**, *77*, 4675. Stiel, H.; Leupold, D.; Teuchner, K.; Nowak, F.; Scheer, H.; Cogdell, R. J. *Chem. Phys. Lett*. **1997**, *276*, 62.

(11) Freiberg, A.; Jackson, J. A.; Lin, S.; Woodbury, N. W. *J. Phys. Chem. A* **1998**, *23*, 4372.

(12) Lin, X.; Murchison, H. A.; Nagarajan, V.; Parson, W. W.; Allen, J. P.; Williams, J. C. *Proc. Natl. Acad. Sci. U.S.A.* **1994**, *91*, 10265.

(13) Fidder, H.; Knoester, J.; Wiersma, D. A. *J. Chem. Phys.* **1991**, *95*, 7880.

(14) Reddy, N. R. S.; Picorel, R.; Small, G. J. *J. Phys. Chem*. **1992**, *96*, 6458.

(15) Hu, X.; Ritz, T.; Damjanovic, A.; Schulten, K. *J. Phys. Chem. B* **1997**, *101*, 3854. Hu, X.; Schulten, K. *Phys. Today* **1997**, *8*, 28.

(16) Struve, W. In *Anoxygenic Photosynthetic Bacteria*; Blankenship, R. E., Madigan, M. T., Bauer, C. E., Eds.; Kluwer Academic Publishers: Dordrecht, 1995; pp 297−313.

(17) Juzeliunas, G. *Z. Phys. D* **1988**, *8*, 379.

(18) Liuolia, V.; Valkunas, L.; van Grondelle, R. *J. Phys. Chem. B* **1997**, *101*, 7343.

(19) Davydov, A. S. *Theory of Molecular Excitons*; Plenum Press: New York, 1971.

(20) There is a misprint in ref 18. Equation 8 of ref 18 should read $E_\nu(k) = (\Delta_1 + \Delta_2)/2 - (-1)^\nu\{[(\Delta_1 - \Delta_2)/2]^2 + |L_{12}(k)|^2\}^{1/2}$.

(21) Novoderezhkin, V. I.; Razjivin, A. P. *Photosynth. Res.* **1994**, *42*, 9.

(22) Monshouwer, R.; Abrahamsson, M.; van Mourik, F.; van Grondelle, R. *J. Phys. Chem. B* **1997**, *101*, 7241.

(23) Wu, H.-M.; Rätsep, M.; Jankowiak, R.; Cogdell, R. J.; Small, G. J. *J. Phys. Chem. B* **1997**, *101*, 7641. Wu, H.-M.; Rätsep, M.; Lee, I.-J.; Cogdell, R. J.; Small, G. J. *J. Phys. Chem. B* **1997**, *101*, 7654.

(24) Freiberg, A.; Lin, S.; Timpmann, K.; Blankenship, R. E. *J. Phys. Chem. B* **1997**, *101*, 7211.

(25) Dracheva, T. V.; Novoderezhkin, V. I.; Razjivin, A. P. *Photosynth. Res.* **1996**, *49*, 269.

(26) Jimenez, R.; Dikshit, S. N.; Bradforth, S. E. Fleming, G. R. *J. Phys. Chem*. **1996**, *100*, 6825.

(27) Chachisvilis, M.; Pullerits, T., Sundström, V. *J. Phys. Chem*. **1997**, *101*, 7275.

(28) Knapp, E. W. *Chem. Phys*. **1984**, *85*, 73.

(29) Meier, T.; Zhao, Y.; Chernyak, V.; Mukamel, S. *J. Chem. Phys.* **1997**, *107*, 3876.

(30) Godik, V. I.; Timpmann, K.; Freiberg, A.; Moskalenko, A. A. *FEBS Lett*. **1993**, *327*, 68.

(31) Leegwater, J. A. *J. Phys. Chem*. **1996**, *100*, 14403.

(32) Schreiber, M.; Toyozava, Y. *J. Phys. Soc. Jpn.* **1982**, *51*, 1528.

(33) Freiberg, A.; Saari, P. *IEEE J. Quantum Electron*. **1983**, *19*, 622.